MNRAS **000**, 000–000 (0000) Preprint 3 November 2015 Compiled using MNRAS LATEX style file v3.0

Population statistics of beamed sources-III: Intrinsic probability density functions in the time domain

I.Liodakis[1,2]⋆ and V. Pavlidou[1,2]
[1]*Department of Physics and ITCP†, University of Crete, 71003, Heraklion, Greece*
[2]*Foundation for Research and Technology - Hellas, IESL, Voutes, 7110 Heraklion, Greece*

arXiv:1511.00434v1 [astro-ph.HE] 2 Nov 2015

3 November 2015

ABSTRACT
In a companion paper we have constructed a new statistical model for blazar populations, which reproduces the apparent velocity and redshift distributions from the MOJAVE survey while assuming single power law distributions for the Lorentz factors and the unbeamed monochromatic radio luminosity. Treating two separate cases, one for the BL Lac objects (BL Lacs) and one for the Flat Spectrum Radio Quasars (FSRQs), we calculated the distribution of the timescale modulation factor $\Delta t'/\Delta t$ which quantifies the change in observed timescales compared to the rest-frame ones due to redshift and relativistic compression. We found that $\Delta t'/\Delta t$ follows an exponential distribution with a mean depending on the flux limit of the sample, for both classes. In this work we produce the mathematical formalism that allows us to use this information in order to uncover the underlining rest-frame probability density function (PDF) of observable/measurable timescales of blazar jets, by fitting their observed probability density function. We test our proposed methodology extensively using simulated data, and identify limits of applicability and potential biases due to observational systematics and sample selection.

Key words: galaxies: active – galaxies: jets – galaxies: blazars

1 INTRODUCTION

Blazars are among the most active of galaxies with jets pointed close to our line of sight. Their jets are known to show unique properties, such as superluminal motion, boosted emission, and high variability throughout the entire electromagnetic spectrum from γ-rays to radio. These unique properties are attributed to the preferential alignment of their jet (Blandford & Königl 1979). Due to beaming, small differences in the rest frame result in large scatter of observables, hampering phenomenological studies and dispersing correlations and behavior trends. This also constitutes the reason why there are still many questions regarding blazars awaiting answers, despite many years of systematic study. Even today very little is known about blazar properties in their rest frame. In this work we focus on the time domain of blazar jets.

Timescales in blazars are compressed due to Doppler boosting, but are also elongated due to the expansion of the Universe. This distortion is quantifiable by the timescale modulation factor (Eq. 1):

$$\frac{\Delta t'}{\Delta t} = \frac{1+z}{D}, \tag{1}$$

where $\Delta t'$ is in the observer's frame, Δt in the rest frame of the jet, z is the redshift and D is the Doppler factor. Even though redshift is, in most cases, a well measured quantity, acquiring the amount of boosting in a jet is not straight forward (Liodakis & Pavlidou 2015b). Although several methods have been proposed (e.g. Ghisellini et al. 1993; Readhead 1994; Lähteenmäki & Valtaoja 1999), the amount of available data in the literature is limited, making a more broad statistical study unfeasible. In addition, Doppler factor estimates involve large uncertainties (Liodakis & Pavlidou 2015b), so "correcting" the measured timescales may in fact introduce even more dispersion in the distribution of observables. In order to overcome such limitations, we have created a model which can recover boosting not in *individual* objects, but rather in a population, by recovering the Doppler factor distribution of flux-limited samples.

Understanding the intrinsic spread of events in the time domain can undoubtedly provide us with important information regarding a plethora of physical processes in blazars. It will also allow us to probe correlations between differ-

⋆ liodakis@physics.uoc.gr
† Institute for Theoretical and Computational Physics, formerly Institute for Plasma Physics

© 0000 The Authors

ent emission regions, test emission and jet models, as well as distinguish between different mechanisms responsible for time-domain phenomena such as the rotations of the EVPA (Electric Vector Position Angle) (Blinov et al. 2015) present in blazars.

This paper is organized as follows. In §2 we describe our model for the blazar population. In §3 we present our mathematical formalism for six different families of intrinsic probability density functions. In §4 we benchmark our method with respect to cadence of observations and sample size, and in §5 the conclusions derived from this work.

The cosmology we have adopted throughout this work is $H_0 = 71\ \mathrm{km\,s^{-1}\,Mpc^{-1}}$, $\Omega_m = 0.27$ and $\Omega_\Lambda = 1 - \Omega_m$ (Komatsu et al. 2009).

2 BLAZAR POPULATION MODEL

Although blazars can exhibit different behaviors on a source-by-source basis, they can be statistically treated as a population. Previous population models (see e.g Urry & Padovani 1991; Padovani & Urry 1992; Vermeulen & Cohen 1994; Lister & Marscher 1997) fitted the observed luminosity, and flux-density curves. Because blazars are known to show high variability throughout the electromagnetic spectrum, flux-density can be an unreliable observable.

For this reason, we have opted to use observables that are not affected by variability: the observed apparent velocity and redshift distributions of the MOJAVE (Monitoring Of Jets in Active galactic nuclei with VLBA Experiments)[1] sample (Lister & Homan 2005; Lister et al. 2009, 2013). MOJAVE uses a statistically complete (Lister & Homan 2005) flux density limited sample, ideal for population studies.

We assumed single power-law distributions for the Lorentz factor and the unbeamed luminosity for the simulated parent population. We treated BL Lacs and the FSRQs as separate cases in order to assess the difference in beaming between the two classes. We adopted pure luminosity evolution (Padovani & Urry 1992), where sources become brighter with look-back time while maintaining a constant comoving volume density, making the number of sources in any redshift bin proportional to the comoving volume element in that bin ($dn \propto dV$). For every simulated source we used a Monte-Carlo approach to calculate the simulated observable distributions: we drew values for the intrinsic luminosity L_ν, viewing angle θ_j, and Lorentz factor Γ; calculated a flux density (Eq.2),

$$S_\nu = \frac{L_\nu D^p}{4\pi d_L^2}(1+z)^{1+a}, \tag{2}$$

where d_L is the luminosity distance, a the spectral index, and p is defined as $p = 2 - a$; and we then applied the 1.5 Jy flux-limit of the MOJAVE sample which served as a constrain between simulated beamed and unbeamed sources.

Following the procedure described above, we were able to produce simulated samples for the blazar populations, from which we extracted information regarding the Doppler factors, beaming between different sources in a flux-limited sample and the distribution of the timescale modulation factor in each class. We have found that the timescale modulation factor follows an exponential distribution (Eq. 3) for both classes with almost identical means (0.281 for the BL Lacs and 0.277 for the FSRQs, for 1.5 Jy flux-limited samples),

$$P(m) = C(\lambda e^{-\lambda m}), \tag{3}$$

where $m = (1+z)/D$ (Eq. 1), C is a normalization constant to account for the truncated range and λ is the inverse mean of the distribution.

For a more detailed description of the model, results and applications see Liodakis & Pavlidou 2015a (hereafter Paper I), and Liodakis & Pavlidou (2015b).

[1] http://www.physics.purdue.edu/MOJAVE/

3 INTRINSIC PROBABILITY DENSITY FUNCTION OF TIMESCALES

Our aim in this work is to extract information about the intrinsic (rest-frame) probability density function (pdf) of timescales for any class of events characterized by a single timescale per blazar. In order to achieve this, we first treat the inverse problem: given a rest-frame pdf of timescales in the blazar population for events of a particular class, what would be the *observed* timescale pdf, after applying the modulation induced by relativistic effects?

Assuming that the physical processes in the rest frame have no knowledge of redshift or Doppler factor and are completely independent of the observer, the intrinsic timescales of any event are independent of the timescale modulation factor $m = (1+z)/D$. As a result,

$$P(t_i|m) = P(t_i)P(m), \tag{4}$$

where the $P(t_i|m)$ is the probability of observing t_i given m, $P(t_i)$ is the intrinsic timescale probability density, and $P(m)$ is the timescale modulation factor probability density (Eq. 3). The observed timescales (t_o) are connected to the intrinsic (t_i) through $t_o = mt_i$. Thus Eq. 4 can be transformed as:

$$P(t_o, m) = P(t_i, m)|J(t_i, m)|, \tag{5}$$

where $J(t_i, m)$ is the Jacobian of the transformation. From the relation between observed and intrinsic timescales, the Jacobian will be:

$$J(t_i, m) = \begin{bmatrix} \frac{1}{m} & 0 \\ 0 & 1 \end{bmatrix} \tag{6}$$

Thus the determinant of Jacobian is equal to:

$$|J(t_i, m)| = \frac{1}{m}, \tag{7}$$

and Eq.5 becomes,

$$P(t_o, m) = P(t_i)P(m)\frac{1}{m}. \tag{8}$$

The probability density function of the observed timescales is thus:

$$P(t_o) = \int_{m_{min}}^{m_{max}} P(t_o, m)dm = \int_{m_{min}}^{m_{max}} P(t_i)C(\lambda e^{-\lambda m})\frac{1}{m}dm, \tag{9}$$

where C is the normalization constant and m_{min}, m_{max} are the minimum and maximum timescale modulation factors.

Since we know $P(m)$ from the results of Paper I, we can assume a family of distributions for $P(t_i)$ and use Eq. 9 to obtain the resulting $P(t_o)$. The parameters of $P(t_i)$ can be optimized by requiring that the resulting $P(t_o)$ fits the observed data best. In this work we will provide some examples of this process for the most commonly used and/or encountered distributions in astrophysics in general.

3.1 Intrinsic Delta Function Distribution

If the intrinsic timescale distribution is a Delta function (all events share the same duration in the rest frame in all blazars) in the form of $\delta(t_i - \frac{t_o}{m})$, where t_i is the characteristic timescale of the δ-function, Eq. 9 becomes:

$$P(t_o) = \int_{m_{min}}^{m_{max}} \delta(t_{i,o} - \frac{t_o}{m}) C(\lambda e^{-\lambda m}) \frac{1}{m} dm. \quad (10)$$

In order to solve the integral we have to transform $\delta(t_{i,o} - \frac{t_o}{m})$ to $\delta(m - \frac{t_o}{t_{i,o}})$ taking into account that, in general,

$$\delta(g(x)) = \frac{\delta(x - x_0)}{|g'(x)|_{x_0}|}. \quad (11)$$

In our case $g(m) = t_i - \frac{t_o}{m}$ and $\delta(m - x_0) = \delta(m - \frac{t_o}{t_{i,o}})$. From Eq. 11 we have:

$$\delta(t_{i,o} - \frac{t_o}{m}) = \frac{t_o}{t_i^2} \delta(m - \frac{t_o}{t_i}) \quad (12)$$

The probability density function of the observed timescales will be:

$$\begin{aligned} P(t_o) &= \int_{m_{min}}^{m_{max}} \frac{t_o}{t_i^2} \delta(m - \frac{t_o}{t_i}) C(\lambda e^{-\lambda m}) \frac{1}{m} dm \\ &= \frac{C\lambda}{t_i} e^{-\lambda(t_o/t_i)}. \end{aligned} \quad (13)$$

The value of C can be calculated as a function of t_i and t_{min}, t_{max} (the bounds of the observed timescales) by requiring $P(t_o)$ to be normalized:

$$C = \frac{1}{t_i [e^{-\lambda t_{min}/t_i} - e^{-\lambda t_{max}/t_i}]}. \quad (14)$$

Thus the probability density function will be:

$$P(t_o) = \frac{\lambda e^{-\lambda(t_o/t_i)}}{t_i [e^{-\lambda t_{min}/t_i} - e^{-\lambda t_{max}/t_i}]}. \quad (15)$$

Equation 15 can be fitted to the observed data, in order to optimize the characteristic timescale t_i of the intrinsic δ-function

3.2 Intrinsic Uniform Distribution

If all timescales in blazar jets in the rest-frame are equally probable, we can assume an intrinsic uniform distribution in the form of:

$$P(t_i) = \begin{cases} \frac{1}{t_{i,max} - t_{i,min}}, & t_{i,min} \le t_i \le t_{i,max} \\ 0, & t_i \le t_{i,min} \text{ or } t_i \ge t_{i,max} \end{cases} \quad (16)$$

Using the Heaviside step function defined as:

$$H(x) = \begin{cases} 0, & x < 0 \\ 1, & x > 0 \end{cases} \quad (17)$$

we can re-write Eq. 16:

$$\begin{aligned} P(t_i) &= \frac{1}{t_{i,max} - t_{i,min}} H(t_i - t_{i,min}) H(t_{i,max} - t_i) \\ &= \frac{1}{t_{i,max} - t_{i,min}} H(\frac{t_o}{m} - t_{i,min}) H(t_{i,max} - \frac{t_o}{m}). \end{aligned} \quad (18)$$

Then Eq. 9 becomes:

$$\begin{aligned} P(t_o) &= \frac{C\lambda}{t_{i,max} - t_{i,min}} \int_{m_{min}}^{m_{max}} \frac{1}{m} e^{-\lambda m} \\ &\times H(\frac{t_o}{m} - t_{i,min}) H(t_{i,max} - \frac{t_o}{m}) dm. \end{aligned} \quad (19)$$

Due to the properties of the Heaviside step function (Eq. 17) the observed probability density will be non-zero for $\frac{t_o}{m} - t_{i,min} > 0 \Rightarrow m < \frac{t_o}{t_{i,min}}$ and $t_{i,max} - \frac{t_o}{m} > 0 \Rightarrow m > \frac{t_o}{t_{i,max}}$. For the bounds of the integral there are four cases, two for the upper and two for the lower bound. For the upper bound either $m_{max} > \frac{t_o}{t_{i,min}}$ and the bound is $\frac{t_o}{t_{i,min}}$, or $m_{max} < \frac{t_o}{t_{i,min}}$ and the bound is m_{max}. For the lower bound either $m_{min} > \frac{t_o}{t_{i,max}}$ and the lower bound is m_{min}, or $m_{min} < \frac{t_o}{t_{i,max}}$ and the lower bound is $\frac{t_o}{t_{i,max}}$:

If $m_{max} < \frac{t_o}{t_{i,min}}$ then:

$$P(t_o) = \begin{cases} \frac{C\lambda}{t_{i,max} - t_{i,min}} \int_{m_{min}}^{m_{max}} \frac{1}{m} e^{-\lambda m} dm, & t_o \le t_{i,max} m_{min} \\ \frac{C\lambda}{t_{i,max} - t_{i,min}} \int_{t_o/t_{i,max}}^{m_{max}} \frac{1}{m} e^{-\lambda m} dm, & t_o \ge t_{i,max} m_{min} \end{cases} \quad (20)$$

If $m_{max} > \frac{t_o}{t_{i,min}}$ then:

$$P(t_o) = \begin{cases} \frac{C\lambda}{t_{i,max} - t_{i,min}} \int_{m_{min}}^{t_o/t_{i,min}} \frac{1}{m} e^{-\lambda m} dm, & t_o \le t_{i,max} m_{min} \\ \frac{C\lambda}{t_{i,max} - t_{i,min}} \int_{t_o/t_{i,max}}^{t_o/t_{i,min}} \frac{1}{m} e^{-\lambda m} dm, & t_o \ge t_{i,max} m_{min} \end{cases} \quad (21)$$

Fitting Eq. 20 and 21 to the observed data, we can optimize for $t_{i,min}$ and $t_{i,max}$ that enter Eq. 18.

3.3 Intrinsic Power Law Distribution

We now assume that the intrinsic timescales in all blazars follow a power law distribution with slope k in the form of:

$$P(t_i) = C_1 t_i^k H(t_i - t_{i,min}) H(t_{i,max} - t_i). \quad (22)$$

$H(t_i - t_{i,min})$ and $H(t_{i,max} - t_i)$ are Heaviside step functions (Eq. 17) in order to account for the truncated range of the intrinsic timescales. Equation 9 becomes:

$$P(t_o) = \int_{m_{min}}^{m_{max}} C_1 (\frac{t_o}{m})^k H(\frac{t_o}{m} - t_{i,min}) H(t_{i,max} - \frac{t_o}{m}) C(\lambda e^{-\lambda m}) \frac{1}{m} dm \quad (23)$$

Setting $C_2 = C_1 C$, and following the procedure described in §3.2:

If $m_{max} < \frac{t_o}{t_{i,min}}$ then:

$$P(t_o) = \begin{cases} C_2 \lambda t_o^k \int_{m_{min}}^{m_{max}} \frac{1}{m^{k+1}} e^{-\lambda m}, & t_o \le t_{i,max} m_{min} \\ C_2 \lambda t_o^k \int_{t_o/t_{i,max}}^{m_{max}} \frac{1}{m^{k+1}} e^{-\lambda m}, & t_o \ge t_{i,max} m_{min} \end{cases} \quad (24)$$

If $m_{max} > \frac{t_o}{t_{i,min}}$ then:

$$P(t_o) = \begin{cases} C_2 \lambda t_o^k \int_{m_{min}}^{t_o/t_{i,min}} \frac{1}{m^{k+1}} e^{-\lambda m}, & t_o \le t_{i,max} m_{min} \\ C_2 \lambda t_o^k \int_{t_o/t_{i,max}}^{t_o/t_{i,min}} \frac{1}{m^{k+1}} e^{-\lambda m}, & t_o \ge t_{i,max} m_{min} \end{cases} \quad (25)$$

We can thus fit a function of the form given in equations 24 and 25 to the observed data to obtain the optimals k, $t_{i,min}$, and $t_{i,max}$ that enter Eq. 22.

3.4 Intrinsic Exponential Distribution

Assuming that the intrinsic timescales in blazar jets follow an exponential distribution in the form of:

$$P(t_i) = C_3 \nu e^{-\nu t_i}, \tag{26}$$

where C_3 is the normalization constant, and ν is the inverse mean of the distribution, equation 9 becomes:

$$P(t_o) = C C_3 \nu \lambda \int_{m_{min}}^{m_{max}} \frac{1}{m} \exp[-(\lambda m + \nu t_o/m)]\, dm \tag{27}$$

Fitting Eq. 27 to the observed data we can optimize ν that enters Eq. 26.

3.5 Intrinsic Normal and Log-Normal Distributions

Assuming that the intrinsic timescales in all blazars are normally distributed with mean μ, and standard deviation σ in the form of:

$$P(t_i) = \frac{1}{\sigma\sqrt{2\pi}} \exp\left[-\frac{(t_i-\mu)^2}{2\sigma^2}\right], \tag{28}$$

equation 9 becomes:

$$\begin{aligned} P(t_o) &= C\lambda \int_{m_{min}}^{m_{max}} \frac{1}{\sigma\sqrt{2\pi}} \exp\left[-\frac{(\frac{t_o}{m}-\mu)^2}{2\sigma^2} - \lambda m\right] \frac{1}{m} dm \\ &= \frac{C\lambda}{\sigma\sqrt{2\pi}} \int_{m_{min}}^{m_{max}} \exp\left[-\frac{(\frac{t_o}{m})^2 + \mu^2 - 2\mu\frac{t_o}{m}}{2\sigma^2} - \lambda m\right] \\ &\times \frac{1}{m} dm. \end{aligned} \tag{29}$$

If the logarithm of the intrinsic timescales is normally distributed with mean $\tilde{\mu}$ and scale σ_{sc} then:

$$P(t_i) = \frac{1}{t_i \sigma_{sc}\sqrt{2\pi}} \exp\left[-\frac{(\ln t_i - \tilde{\mu})^2}{2\sigma_{sc}^2}\right], \tag{30}$$

The probability density function of observed timescales will be:

$$\begin{aligned} P(t_o) &= \frac{C\lambda \exp\left[-\frac{(\ln t_o - \tilde{\mu})^2}{2\sigma_{sc}^2}\right]}{t_o \sigma_{sc}\sqrt{2\pi}} \\ &\times \int_{m_{min}}^{m_{max}} \exp\left[-\frac{(\ln m)^2 + 2\ln m(\tilde{\mu} + \ln t_o)}{2\sigma_{sc}^2} - \lambda m\right] dm \end{aligned} \tag{31}$$

By fitting equations 29 and 31 to the observed data we can optimize for the mean (μ) and standard deviation (σ) entering Eq. 28 and the mean ($\tilde{\mu}$) and scale (σ_{sc}) entering Eq. 30.

The derivation of an analytical solution was only possible for the case of the δ-function. The rest of the cases have to be solved either numerically or with the use of Monte-Carlo sampling.

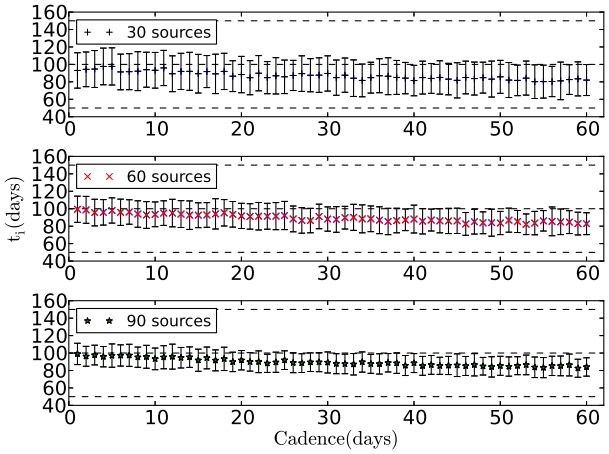

Figure 1. Estimated best-fit t_i versus cadence (both in days) for the "systematic-free" samples. The black "+" is for the 30 source sample, red "x" for the 60 source sample and the green "⋆" for the 90 source sample. The error bars represent the uncertainty of the best-fit t_i.

4 METHOD APPLICATION AND BENCHMARKING

In order to test the accuracy of our method under realistic observing conditions, we generated a simulated survey and explored the accuracy of the method with respect to cadence and sample size.

4.1 Simulated sample

For our benckmarking experiments, we have chosen to use the simple case where all blazars in the rest-frame have the same intrinsic characteristic timescale. Then the rest-frame distribution can be described by a δ-function (Eq. 15). We constructed our simulated samples by drawing a random value for the timescale modulation factor and multiplying it by the intrinsic characteristic timescale which we arbitrarily set to 100 days. The value for the timescale modulation factor was drawn from an exponential distribution (Eq. 3). The mean of the exponential distribution was set to 0.28 for simplicity[2](see §2). In paper I, we found that the maximum compression of timescales is of the order of $\sim 10^{-2}$, so in our experiment we reject any value lower than 10^{-2} and we appropriately renormalize the distribution.

4.2 Benchmarking

The distribution of observed timescales will inevitably have a cut-off at the lower end according to the cadence of our survey. In addition, the measured observer-frame timescale will lay between the actual value and that value minus two times the time interval (Δt) between observations (if, in the worst case scenario, both the beginning/end of an "event" happen exactly after/before the first/last datapoints). For

[2] Although the mean of the exponential depends on the population and flux-limit, it makes no difference for this particular exercise.

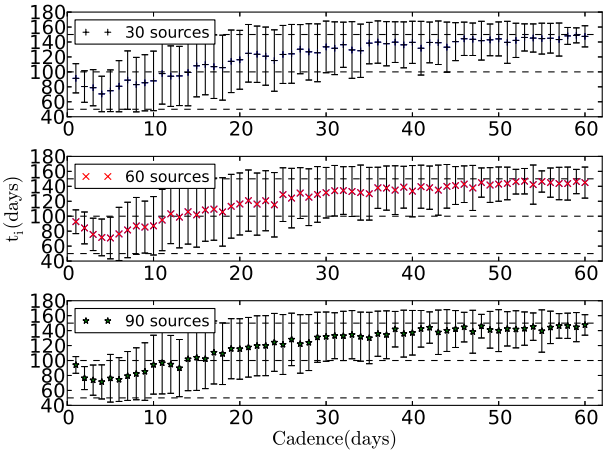

Figure 2. Estimated best-fit t_i versus cadence (both in days) for the "systematics-affected" samples. The black "+" is for the 30 source sample, red "x" for the 60 source sample and the green "⋆" for the 90 source sample. The error bars represent the uncertainty of the best-fit t_i.

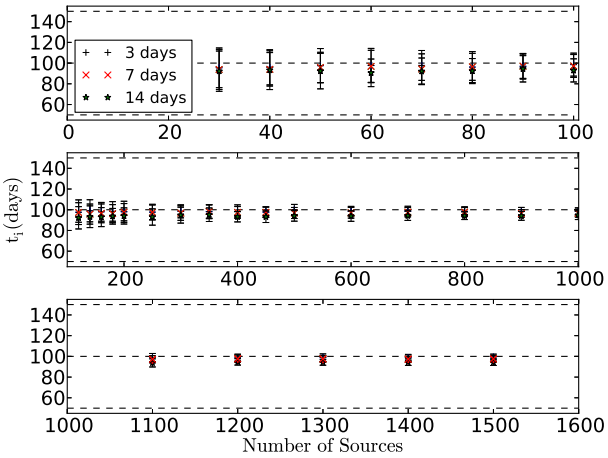

Figure 3. Estimated best-fit t_i versus sample size. The upper panel is for sample size ranging from 30 to 100 sources, middle panel from 100 to 1000 sources, and the lower panel from 1000 to 1500 sources. The black "+" is for the 3 day cadence, red "x" for the 7 day cadence and the green "⋆" for the 14 day cadence. The error bars represent the uncertainty of the best-fit t_i.

this reason, once we generate our simulated sample, we created an "observed" sample by drawing a random value from a uniform distribution with range $[\tau - 2\times\Delta t, \tau]$, where τ is the actual value of the observer-frame timescale.

We treated two different cases. In the first case, the observed distribution is free of systematic errors. Every timescale smaller than Δt is rejected as not observed. In the second case all the timescales smaller than Δt are set as observed, with value equal to that of Δt. Physically, the later case corresponds to observations of events of various timescales (e.g flares in a particular frequency), of which we pick the "fastest". In this scenario faster-than-observed events may occur in a particular source, but the "fastest" one

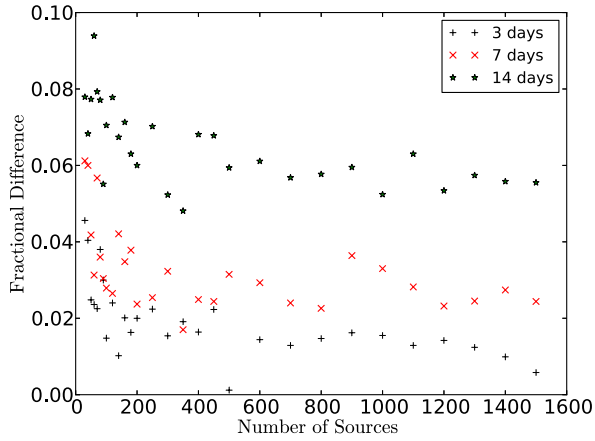

Figure 4. Fractional difference between the estimated best-fit and the "true" t_i versus sample size. The black "+" is for the 3 day cadence, red "x" for the 7 day cadence and the green "⋆" for the 14 day cadence.

we record is set by the survey cadence, leading to systematic offset in our statistical results.

We performed our benchmarking experiments in the following steps:

- We generated an "observed" sample using the procedure described above for a given cadence.
- We constructed the cumulative distribution function of Eq. (15) for different assumed values of t_i and compared it with the simulated "observed" sample with the use of the Kolmogorov Smirmov test (K-S test). The K-S test provided a straightforward way of rejecting distributions that were inconsistent with our simulated dataset.

In order for our distribution to be normalized in the observer's frame, t_{min} was set to the shortest observed value, and t_{max} was set to the total length of the simulated survey, which we set to ten times the longest observed timescale to ensure the survey would be able to detect even the longest of timescales. The value of t_i which yielded the highest p-value of the K-S test was the value we considered the best-fit parameter value.

- We repeated the above process 100 times in order to evaluate the statistical spread of the method, for a given sample size and cadence. We quote the mean of these best-fit parameters as the best-estimated rest-frame timescale and the standard deviation of the estimates in different iterations, as the uncertainty of the final estimate.

Due to relativistic compression, the shortest rest-frame timescale can be either equal or longer than the shortest observed. The longest rest-frame timescale can be up to the maximum observed divided by the maximum relativistic compression ($\sim 10^{-2}$). Thus in the application of the method, the range of the parameter space should be at least from the shortest to 100 times the longest observed timescale. For this particular exercise, since we have a priori knowledge of the t_i, the range is set from 50 to 150 days. If any of the best-fit t_i is ≤ 50 or ≥ 150, this would correspond to a 50% error in the estimate.

We examined three sample sizes (30, 60, 90 sources) and

cadence starting from 1 day, up to 60 days with a step of 1 day. For the first case (systematics-free) we draw sources until we reach the desired sample size in the observer's frame after the cadence limit is applied.

Figure 1 shows the estimated best-fit t_i versus cadence for both cases. The error bars are the spread of the estimated rest-frame timescale. It is clear that increasing the number of sources in our samples results in a more narrow spread of estimates. There is a systematic shift towards lower values of the estimated intrinsic characteristic timescale with the increase of the number of days in cadence. In many cases above 30 days cadence, the best-fit estimate is more than 1σ away from the true value. This shift can be attributed to the fact that, the large number of days in cadence is biasing the sample towards shorter timescales. All of the above is leading us to the conclusion that for a cadence of more than 30 days (~1/3 the actual timescale we are trying to measure), the method is beginning to lose its ability to accurately estimate the best-fit parameter of the intrinsic probability density function.

For the second case (with systematic errors), it is clear from Fig. 2, that introducing systematic errors results in a significantly larger scatter in the estimated best-fit t_i. There are also cases (samples produced with large number of days in cadence) where the estimated best-fit parameter is $t_i \approx 150$ (Fig. 2), which is the upper end of the parameter space. This means that these estimates have a $\gtrsim 50\%$ error. This effect is to be expected, since we are polluting our simulated samples with longer timescales according to the chosen cadence. Moreover, the majority of cases has their 1σ error reaching that level regardless of cadence. We have to conclude that the presence of systematic errors prevents the method from providing an accurate estimate and will lead to the overestimation of the intrinsic timescales.

In addition, we explored the effect of the size of the sample at a fixed cadence. We follow the procedure described above with the difference that this time the cadence is fixed to a predefined value, and the number of sources in the sample varies. We chose three values for the cadence; 3, 7, and 14 days, since any cadence above 30 days results in $> 1\sigma$ departure from the "true" intrinsic timescale (Fig. 1). The different samples had a size starting from 30 sources up to 100 with a 10 source step, from 100 up to 200 with a 20 source step, from 200 up to 500 with a 50 source step, and from 500 up to 1500 with a 100 source step.

Figures 3 shows the estimated t_i versus the sample size with the error bars being the uncertainty of the method, and Fig. 4 the fractional difference of the estimated best-fit and the "true" t_i versus sample size. It is obvious that the larger the sample the smaller the spread (Fig 3), and the better the accuracy of the method (Fig. 4). Regardless of sample size, the method has an accuracy of $\leq 10\%$ error in the estimates (Fig. 4). For samples with size ≥ 200 sources the method can estimate the intrinsic characteristic timescale with a $\leq 8\%$ error for all cadences. Especially for the 3 and 7 day cadence (for samples with size ≥ 200 sources), all the estimates of our method have a $\leq 4\%$ error. For a large number of sources (≥ 200) and high cadence (3 days, i.e 3% of the timescale we are trying to determine) the error of the method is $\sim 1\%$.

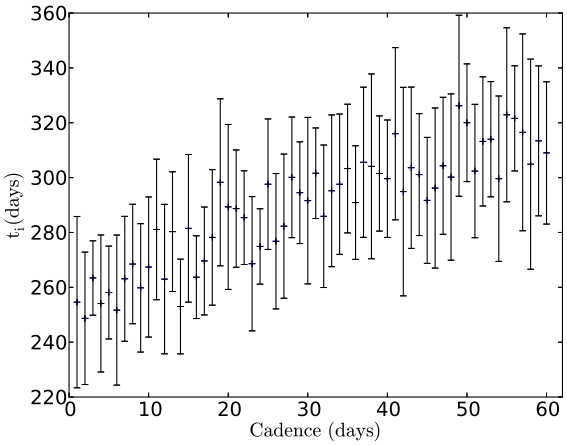

Figure 5. Estimated δ-function best-fit parameter (t_i) for an intrinsic uniform distribution versus cadence. The error bars represent the uncertainty of the best-fit t_i.

4.3 Testing for the type of distribution

The best-fit intrinsic distribution family need not be unique. Different families of distributions of intrinsic timescales can produce similar results in the observer's frame. For example, an intrinsic sharp distribution, would appear consistent with a δ-function as well as with a narrow normal distribution. Physically this is not necessarily problematic, since all the well-fitting distributions should describe approximately the same physical reality (in our example, a "preferred" timescale in the rest-frame). A more worrisome situation would be if, because of uncertainties or systematic effects, a single dataset appeared consistent with families of distributions describing a very different physical reality. To demonstrate how this effect can cause confusion, we tested whether a finite-width intrinsic distribution can appear consistent with a δ-function. To this end, we performed the following experiment. We created simulated samples using an intrinsic uniform distribution from 50 to 500 days. The sample size was fixed to 200 sources, a size large enough to ensure accurate estimates (as seen in Fig. 4). Using the procedure described in §4 we fitted an intrinsic δ-function for cadences from 1 to 60 days. We assumed no a priori knowledge of the intrinsic distribution or the range of the parameter space. Figure 5 shows the δ-function best-fit parameter t_i versus cadence. All the best-fit estimates of the characteristic timescale fall approximately at the median value of the intrinsic distribution. The K-S test yields a probability of consistency that ranges from 40 to $\leq 70\%$. Although there is a large scatter in the estimates even for a cadence of 1 day, the probability of consistency is high enough for the two datasets to be considered consistent. In this case we could naively assume that all blazars have the same characteristic timescale in the jet rest frame. However, there is a simple test for this particular case that can clarify the value of the intrinsic distribution. If indeed the intrinsic distribution of timescales is a δ-function, or at least a sharp distribution, then by fitting a normal distribution, we should in principle find that the best-fit distribution is very sharp. For simplicity we tested only two cadences, 7 and 30 days. The 7 day cadence was chosen because it is the limit at which the method becomes

extremely accurate ($\leq 4\%$ error) and the 30 day cadence because it is the limit after which the method stops producing reliable results.

For the 7 day cadence we find that the best-fit intrinsic normal distribution would have mean $\mu = 227.5$ and standard deviation $\sigma = 216.3$ with a 90% probability of consistency between samples. For the 30 day cadence the best-fit normal distribution has $\mu = 163.2$ and $\sigma = 235.1$ with a 81% probability of consistency. In both cases the resulting best-fit normal distribution is far from consistent with a δ-function. The fact that they are significantly wider and with more than 20% higher probability of consistency, is a good indicator that the "true" intrinsic distribution is much wider than a δ-function. Such simple tests can provide invaluable insights on the "true" shape of the intrinsic distribution in the application of the method.

5 SUMMARY AND CONCLUSIONS

In Paper I, we found that the timescales of the blazar populations are modulated by an exponential distribution. In this work, assuming that the intrinsic timescales of blazars are independent of redshift and Doppler boosting, we have developed a novel method of uncovering the underlying rest-frame probability density function of a class of events in the time domain of blazar jets using the observer-frame probability density. The independence of rest-frame timescales from redshift and Doppler boosting is not obvious. There may be a dependence on either redshift or Doppler boosting, or both. However such a dependence can best be addressed in a model-dependent fashion (i.e. by testing an explicit model proposing such a relationship). Our formalism can be extended in a straight forward fashion to test such models.

In addition we benchmarked our method in a realistic observing scenario. By creating a simulated survey, we explored the effect of cadence and sample size in the application of the method, by addressing the simplest case, i.e one where all blazars have the same characteristic timescale in the jet rest-frame. We investigated two different cases. In the first case all timescales shorter than the cadence of the survey are rejected as not observed, whereas in the second case we are introducing systematic errors by setting all the rejected timescales equal to the cadence of the survey. For the first case we drew simulated sources until a predefined sample size is reached.

For the case with no systematic errors, we found that, when the interval between observations is longer than 30% of the timescale we try to measure, there is a systematic shift in the estimates that can lead to best-fit parameters deviating more than 1σ from the characteristic timescale. This shift is due to the bias towards shorter timescales induced by the cadence limit. Large intervals between observations are preventing our method from producing robust results.

In the case where our simulated survey has systematic errors (i.e timescales shorter than the cadence of the survey are observed as equal to that cadence), we found that the presences of these systematic errors forces the method to overestimate the intrinsic characteristic timescale (Fig. 2). There is a significantly larger uncertainty in the estimates, and in the majority of cases we cannot constrain the timescale better than at the 50% error level. Since many events in the time domain of blazar jets are connected to the size of the emission region through causality arguments, such an overestimation would also lead to the overestimation of that region's size and induce scatter or create artificial correlations between events in the time domain and physical properties of blazar jets. Thus datasets should be treated with great caution with respect to the cadence of the survey in the application of the method.

Exploring the method's sensitivity to sample size, we found that all estimates for sample sizes ≥ 30 sources have an accuracy of $\leq 10\%$. For large enough samples (≥ 200 sources) and high cadence ($\leq 7\%$ of the intrinsic timescale) the method can estimate the rest-frame characteristic timescale with less than 4% error. Surveys with high cadence and large number of sources such as the Owens Valley Radio Observatory (OVRO)[3] monitoring program (Richards et al. 2011) would make an ideal candidate for the application of our method.

The family of distributions that best fits a particular observer-frame dataset need not be unique. Different families can provide similarly fitting results. A test that can help determine whether our deduced rest-frame distribution is an acceptable description of the physical reality of the source population is to compare the best fits from different families of distributions. All distributions with the same number of parameters should converge to a similar answer (for example, regarding distribution width) if the obtained fit is to be reliable. Distributions with more parameters should converge to the simpler distribution shapes, if the simpler distributions are acceptable descriptions of reality, otherwise the simpler distributions should be rejected

In the case of timescale distributions in different wavelengths (e.g optical, γ-rays), whether the same boosting (Doppler factor) applies is still an open question. Deceleration in the jet from the γ-ray to the radio emission region (Georganopoulos & Kazanas 2003a,b, 2004; Giannios et al. 2009) may result in the underestimation of the intrinsic timescales. If such a deceleration does not exist or its effect is not significant, timescales derived from the Fermi Gamma-Ray Space observatory all sky survey (Acero et al. 2015) will also constitute an ideal dataset due to the high cadence of observations and sample size, although one should keep in mind that a flux-limited sample in γ-rays does not translate into a flux-limited sample in radio (Pavlidou et al. 2012), which is the basis of our population models.

ACKNOWLEDGMENTS

The authors would like to thank Talvikki Hovatta for comments that help improve this work. This research was supported by the "Aristeia" Action of the "Operational Program Education and Lifelong Learning" and is co-funded by the European Social Fund (ESF) and Greek National Resources, and by the European Commission Seventh Framework Program (FP7) through grants PCIG10-GA-2011-304001 "JetPop" and PIRSES-GA-2012-31578 "EuroCal".

[3] http://www.astro.caltech.edu/ovroblazars

REFERENCES

Acero F., et al., 2015, ApJS, 218, 23
Blandford R. D., Königl A., 1979, ApJ, 232, 34
Blinov D., et al., 2015, MNRAS, 453, 1669
Georganopoulos M., Kazanas D., 2003a, ApJ, 589, L5
Georganopoulos M., Kazanas D., 2003b, ApJ, 594, L27
Georganopoulos M., Kazanas D., 2004, New Astron. Rev., 48, 403
Ghisellini G., Padovani P., Celotti A., Maraschi L., 1993, ApJ, 407, 65
Giannios D., Uzdensky D. A., Begelman M. C., 2009, MNRAS, 395, L29
Komatsu E., et al., 2009, ApJS, 180, 330
Lähteenmäki A., Valtaoja E., 1999, ApJ, 521, 493
Liodakis I., Pavlidou V., 2015a, MNRAS, 451, 2434
Liodakis I., Pavlidou V., 2015b, MNRAS, 454, 1767
Lister M. L., Homan D. C., 2005, AJ, 130, 1389
Lister M. L., Marscher A. P., 1997, ApJ, 476, 572
Lister M. L., et al., 2009, AJ, 137, 3718
Lister M. L., et al., 2013, AJ, 146, 120
Padovani P., Urry C. M., 1992, ApJ, 387, 449
Pavlidou V., et al., 2012, ApJ, 751, 149
Readhead A. C. S., 1994, ApJ, 426, 51
Richards J. L., et al., 2011, ApJS, 194, 29
Urry C. M., Padovani P., 1991, ApJ, 371, 60
Vermeulen R. C., Cohen M. H., 1994, ApJ, 430, 467